Improvement of aluminium foaming by powder consolidation under vacuum

C. Jiménez[1], F. Garcia-Moreno[2], M. Mukherjee[2], O. Goerke[3], J. Banhart[1,2]

[1] Technische Universität Berlin, Hardenbergstr. 36, 10623 Berlin, Germany

[2] Helmholtz-Zentrum Berlin für Materialen and Energie, Glienicker Str. 100, 14109 Berlin, Germany

[3] Technische Universität Berlin, Englische Str. 20, 10587 Berlin, Germany

Abstract

Foamable AlSi11 precursors were uni-axially hot-compacted under vacuum and air and then foamed. We studied the influence of the compaction atmosphere on the foaming behaviour in-situ by X-ray radioscopy. In vacuum-pressed precursors the growth of elongated bubbles was reduced, resulting in a larger expansion and more reproducible foaming due to improved consolidation. As a consequence, foams made from these precursors show a more regular pore size distribution than foams made from traditionally pressed precursors.

Keywords: foam; pore size; powder consolidation; foaming; aluminium

The properties of metal foams are influenced by morphological features, in particular by the pore size distribution [1]. Although the exact interrelationship between properties and structure is not fully known, it is assumed that a uniform distribution of pores free of defects is desirable [2].

The powder metallurgical (PM) route is one of the commercially exploited methods to produce aluminium foams [3]. Aluminium powder is mixed with alloying elements, and TiH_2 is added as blowing agent in most cases. The powders are consolidated to yield foamable precursors, after which the foaming process is initiated by heating [4].

Al-Si alloys based on pure Al and Si powders are cost-effective for this manufacturing route. Studies based on microscopy and synchrotron X-ray micro-tomography have shown that in Al-Si precursors pore initiation is spatially

correlated with Si particles. In early stages pores are crack-like, leading to irregularities in the final products [5, 6]. This observation was attributed to the mismatch between the melting of the respective alloy and TiH_2 decomposition. Investigations focused on lower melting aluminium alloys [3, 7, 8] and pre-treated TiH_2 powders [9-12] brought significant progress in producing more regular porous structures. The observed formation of crack-like pores shows that not only the blowing agent decomposes before melting of the alloy, but it also makes evident deficiencies of powder consolidation.

In traditional powder metallurgy hot-compaction under vacuum is a known practice to improve the consolidation of aluminium PM parts [13, 14]. Hence hot-compaction under vacuum could reduce the formation of crack-like elongated pores during foaming.

In order to evaluate this possibility, we compacted AlSi11precursors containing TiH_2 both under vacuum and air. We compared these two types of compacts in terms of properties of the compacted materials, foaming behaviour, hydrogen evolution and resulting foam structure.

We used aluminium (Alpoco Ltd., purity 99.7%), silicon (Wacker Chemie GmbH, purity 99.5%) and TiH_2 (Chemetall GmbH, purity 98.8 %) powders. TiH_2 was pre-treated at 480 °C for 180 minutes in air. We measured the oxygen content of the powders by carrier gas hot extraction and the density by helium pycnometry.
The powders were blended to prepare the alloy AlSi11 + 0.5 wt.% TiH_2.

We prepared tablets of 30 g mass and 36 mm diameter by uni-axial hot-compaction in air and under vacuum inside a chamber. A pre-compaction step was done at 200 °C, applying 300 MPa for 60 s. Hot-compaction was performed at 400 °C applying 300 MPa for 300 s in all cases. The gas pressure was kept below 8×10^{-2} mbar during hot-compaction under vacuum.

A shell of 1 mm thickness was removed from the tablets by machining, after which we determined the densities by Archimedes' principle. We measured the oxygen content of both compacted materials, and examined microstructural features by light and scanning electron microscopy (SEM). After polishing, the surfaces were etched for 5 s in aqueous solution of NaOH (10 g of NaOH in 80 ml of distilled water at 50 °C).

We studied hydrogen evolution from compacted precursor materials as function of time and temperature by mass spectrometry. For this, we prepared cylinder-shaped samples of 5.7 mm diameter×4.7 mm height. We heated the samples in flowing synthetic air (50 $ml.min^{-1}$) inside a tube furnace coupled via a skimmer to a quadrupole mass spectrometer. We heated at 40 $K.min^{-1}$ from 37 °C up to 680 °C, held there for 30 minutes and cooled down (T(t) in Fig. 2).

For foaming, the material was cut to 10×10×3 mm^3 size. The volume-to-surface ratio of these samples is equal to that of the cylinders. For each type of precursor, six identical samples were foamed in air at ambient pressure by heating on a resistive heater (~ 300 W) at 160 $K.min^{-1}$ from 37 °C to 680 °C and holding there for 120 s. After this, the heater was turned off and natural cooling took place (T(t) in Fig. 3 a). Foam temperature was measured by a thermocouple at the bottom of the sample. The foaming process was investigated in-situ by X-ray radioscopy with a time resolution of 2 s and using the image analysis software AXIM [15] to determine area expansion as a function of time.

We characterized non-destructively one representative foam from each group by X-ray tomography, performed in a setup similar to the one used for radioscopy. 1000 projected radiographs were taken for 360° rotation and reconstructed using the software Octopus 8.2. VGStudioMax 1.2.1 was used to extract 3D sections and Avizo 5 for quantitative 3D pore analysis.

The measured oxygen contents of Al, Si and pre-treated TiH_2 powders were 0.46±0.07, 0.22±0.01 and 4.02±0.08 (in wt.%), their densities 2.73±0.07, 2.33±0.05 and 3.76±0.07 (in $g.cm^{-3}$), respectively. From these values, we calculated an oxygen content of 0.45±0.07 wt.% and a density of 2.68±0.06 $g.cm^{-3}$ for the powder mixture. The latter was adopted as theoretical full density for the compacts.

Oxygen contents and relative densities of the compacts are summarized in Table 1. Vacuum-pressed tablets achieved higher relative densities than air-pressed tablets. The oxygen content of vacuum-pressed compacts was almost the same as that of the powder mixture before compaction, whereas pressing in air increased the oxygen level.

The residual porosity in both compacts was mostly located near Si particles. Many Si and TiH_2 particles were fractured after compaction (Fig. 1 a and b).

The specific hydrogen release for “mass = 2” per unit sample mass is given in Fig. 2. The onset of hydrogen release – 343 °C in the air-pressed sample – was shifted by 212 K up to 555 °C in the vacuum-pressed sample. Below each onset, the release increased almost linearly. Vacuum-pressed material released hydrogen at half the rate of air-pressed material. The first peak of hydrogen release in both specimens occurred at 579 °C, the second peak at 663 °C, after which hydrogen release decayed and almost exhausted after 22 minutes.

From the expansion curves in Fig. 3 a, we calculated the maximum area expansion. Vacuum-pressed precursors reached 365±21% maximum area expansion, whereas air-pressed precursors reached 288±30% only. Up to 555 °C, both groups expanded linearly. A first range of non-linear expansion occurred between 555 °C and 647 °C (also indicated in Fig. 2), where the deviation from the initial linear expansion was more pronounced for the vacuum group that started to surpass the air group. Above 647°C, the air group of expansion curves developed a larger scatter than the vacuum group.

We also compared the foaming behaviour in Fig. 3 b using radioscopic image sequences. Both samples were at 37 °C at t = 0, and at 680±5 °C after 245, 280 and 336 s. The expansions of these two representative foams at those times are marked in Fig. 3 a with the full-circle and full-square symbols. Elongated bubbles perpendicular to the compaction direction formed in both kinds of precursors. They initially grew perpendicular to the compaction direction. In air-pressed precursors this growth was more localized, and after 245 s the big elongated bubbles became roundish but evolved to an inhomogeneous structure. On the contrary, in the vacuum-pressed precursor more and smaller elongated bubbles were formed. Their growth perpendicular to the compaction direction eventually stopped and the foam expanded homogeneously after 245 s.

X-rays tomographic sections and 3D pore size distributions of the representative foams are compared in Fig. 4. The sections correspond to the central plane of the foams perpendicular to the compaction direction. The foam made from air-compacted precursor had a large population of small pores and high solid fraction concentrated in the outer region. In comparison, the foam made from vacuum-pressed powder had a smaller population of small pores in the outer region and a more uniform distribution of the solid fraction throughout the section. Structural defects

such as missing cell walls and interconnections between pores were present in both foams.

3D pore analysis was performed and the volume of spherical pores of equivalent diameter *D* calculated, applying a lower threshold of 100 μm. Both pore size distributions were bimodal and fitted with a double-peak Gaussian model. The resulting parameters were included in Fig. 4. The total pore volume of the foam made from air-pressed precursor was 855 mm^3, while that of the foam made from vacuum-pressed precursor was 1172 mm^3. The ratio of these two volumes, 0.73, expresses the improvement in expansion. The ratio between standard deviations of the second peak was $\sigma_{2,air} / \sigma_{2,vacuum} \cong 1.8$. Hence the large pores of the foam made from vacuum-pressed precursor were not only centred at a smaller mean diameter, 2.39 mm, but were much more equally distributed than in the foam made from air-pressed precursor.

Besides the spatial correlation between early crack-like pores and Si particles [5, 6], Helfen et al. concluded that the bonding strength between Al and Si is lower than between Al and TiH_2 or between Al particles [6]. Si and TiH_2 are both brittle. They fracture and host residual porosity inside or nearby them (Fig 1). Strengthening Al/Si or Al/TiH_2 bonds would not improve the resistance of the compacted material to the growth of crack-like pores. The alternative is to strengthening the bonding between Al particles. Al powder is ductile but the powder particles are covered by a stable oxide layer which can also react with moisture to form hydroxides. During hot compaction, Al particles are squeezed and sheared to get metallically bonded. Compaction under vacuum helps removing entrapped gasses, dehydrating oxides and preventing further oxidation [13, 14]. Thus the oxide layers break into smaller pieces and the metallic bonding between Al particles is achieved in larger regions compared to compaction in air. In this manner, we produce a more consolidated Al matrix able to reduce cracking by controlling the growth of crack-like pores formed in the solid state.

The increase in density due to vacuum pressing as given in Table 1 indicates a tendency, but does not reveal to what extent the Al particles are metallically bonded. The oxygen content gives complementary information as it is localized on unbound surfaces. Al PM-parts are degassed typically above 500 °C [13, 14]. Therefore, one possibility to ensure good consolidation of foamable precursors would be to hot-press

at higher temperatures than 400 °C. However, untreated TiH_2 starts to decompose at around 400 °C [11]. Even though TiH_2 is pre-treated in air to retard its decomposition, the particles break after compaction as shown in Fig. 1 b, creating non-oxidised surfaces, thus facilitating decomposition. The release of H_2 in the presence of oxygen can lead to water formation [16, 17], which could be the reason for the increase in oxygen content of the air-pressed compacts.

The hydrogen evolution from compacted material as shown in Fig. 2 was used to evaluate the effect of the compaction atmosphere on consolidation applying a temperature profile similar to the one used for foaming. The difference of 212 K (555 K– 343 K) between onset temperatures confirmed that compaction under vacuum significantly improved consolidation.

According to the binary phase diagram, the first liquid should be formed at the eutectic temperature 577 °C [18]. We observed that at 579 °C hydrogen losses decay (first peak), as if the formation of liquid partially sealed the paths through which hydrogen escaped. The same melting sequence applies for both compacts, which is why the two peaks were observed at the same temperatures. Matijasevic-Lux et al. measured hydrogen evolution from AlSi6Cu4 and von Zeppelin et al. from AlSi7, both containing TiH_2 [11, 19]. Both authors reported single peak structures for hydrogen release rather than the double peak structure we observe. We attribute this difference to the lower heating rates (20 $K.min^{-1}$ and 5 $K.min^{-1}$, respectively) and the smaller sample sizes ($3\times3\times3$ mm^3) used by them. After the first peak has levelled off, hydrogen release approaches a second maximum, as if TiH_2 decomposition becomes dominant in the semi-molten state of the alloy. The second peak at 663°C is close to the melting point of Al (660 °C).

The porous structure is initiated in the solid state and carries a history which cannot be erased by the melting sequence during foaming, as shown in Fig. 3. The better consolidated vacuum-pressed precursors reached larger expansions than air-pressed ones due to the significant reduction of hydrogen losses, especially below the eutectic temperature. The expansion of vacuum-pressed precursors deviated from the initial linear increase at around 555 °C, the temperature at which these precursors release their first hydrogen (Fig. 2). The more abrupt change in hydrogen release and expansion that occurs at 555 °C for the vacuum-pressed material, points at the relationship between onset of hydrogen release and non-linear expansion.

Helfen et al. studied the evolution of the porous structure of AlSi7 using computed tomography [20]. They observed that with the appearance of the liquid, the crack-like interconnected pore morphology gradually rounded off in order to reduce surface tension. This is consistent with our observations that above 647 °C expansion could develop steadily sustained by the decomposition of TiH_2 and a large enough fraction of liquid. The system tended to have more roundish bubbles, but the definite decay of hydrogen release needed the melting sequence to be completed, i.e. to reach the melting point of Al (second peak in Fig. 2).

Shorter and more numerous elongated bubbles in the vacuum-pressed precursors were further evidence for the better consolidation. These compacts permitted the built-up of higher pressures in smaller pores. The initial growth perpendicular to the compaction direction was arrested, leading to more efficient, homogeneous and reproducible expansion. The more regular porous structure obtained after solidification from vacuum-pressed material (shown in Fig. 4) was just consistent with the limited growth of elongated pores at the early stages of expansion. In the case of air-compacted precursors, the lower onset temperature and the larger hydrogen quantity released made expansion more sluggish over the entire foaming course. After melting, big elongated bubbles formed and maintained their anisotropic shape, eventually leading to non-uniform expansion. As hydrogen escaped through the surface, the built-up of pressure in the outer pores was reduced, and so was their ability to grow after melting. Thus the larger hydrogen losses promoted the accumulation of small pores in a denser outer region of the resulting solid porous structure.

In conclusion, hot compaction under vacuum led to better consolidation of foamable AlSi11 precursors by improving the degree of metallic bonding between aluminium particles. The better consolidation retarded hydrogen evolution and reduced losses especially before melting. The vacuum-pressed metallic matrix was more capable to arrest the growth of elongated bubbles. The result was a larger and more homogeneous expansion and a more regular pore size. The foam made from vacuum-pressed powders had a 37 % larger volume than the foam made from air-pressed powders and a narrower pore size distribution.

Acknowledgements to Christian Abromeit for helpful discussions and Andreas Benz for assistance with tomography.

References

[1] H.P. Degischer, A. Kottar, in: H.P. Degischer and B. Kriszt (Eds.), Handbook of Cellular Metals, Wiley-VCH, Weinheim, 2002, pp. 156-178.

[2] U. Ramamurty, A. Paul, Acta Mater. 52 (2004) 869.

[3] F. Baumgärtner, I. Duarte, J. Banhart, Adv. Eng. Mater. 2, (2000) 168.

[4] J. Baumeister, German Patent DE40 18 360, 1990.

[5] U. Mosler, A. Müller, H. Baum, U. Martin, H. Oettel, in: J. Banhart, M. Ashby and N. Fleck (Eds.), Cellular Metals and Metal Foaming Technology, MIT-Verlag, Bremen, 2001, pp. 233-238.

[6] L. Helfen, T. Baumbach, P. Pernot, P. Cloetens, H. Stanzick, K. Schladitz, J. Banhart, App. Phys. Lett. 86 (2005) 231907.

[7] D. Lehmhus, M. Busse, Adv. Eng. Mater. 6 (2004) 391.

[8] H.M. Helwig, J. Banhart, H. W. Seeliger, German patent application 102008027 798.3, 2008.

[9] A.R. Kennedy, Scripta Mater. 47 (2002) 763.

[10] D. Lehmhus, G. Rausch, Adv. Eng. Mater. 6 (2004) 313.

[11] B. Matijasevic-Lux, J. Banhart, S. Fiechter, O.Görke, N. Wanderka, Acta Mater. 54 (2006) 1887.

[12] B. Matijasevic, J. Banhart, Scripta Mater. 54 (2006) 503.

[13] J.R. Pickens, J. Mater. Sci. 16 (1981) 1437.

[14] J.L. Estrada, J. Duszczyk, B.M. Korevaar, J. Mater. Sci. 26 (1991) 1431.

[15] F. Garcia-Moreno, M. Fromme, J. Banhart, Adv. Eng. Mater. 6 (2004) 416.

[16] L. Schlapbach, in: L.Schlapbach (Ed.), Hydrogen in Intermetallic Compounds II, Springer-Verlag, Berlin Heidelberg New York, 1992, p. 17

[17] V.A. Lavrenko, V.Zh. Shemet, L.A. Petrov, O.A. Teplov, Oxidation of Metals, 33 (1990) 177.

[18] J.L. Murray, A.J. MacAllister. In: H. Baker (Ed.), ASM Handbook, Vol. 3: Alloy Phase Diagrams, ASM International, Materials Park, Ohio, 1999. p. 85

[19] F. von Zeppelin, M. Hirscher, H. Stanzick, J. Banhart, Compos. Sci. Technol 63 (2003) 2293.

[20] L. Helfen, T. Baumbach, H. Stanzick, J. Banhart, Adv. Eng. Mater. 4 (2002) 808.

Figure(s)
Click here to download high resolution image

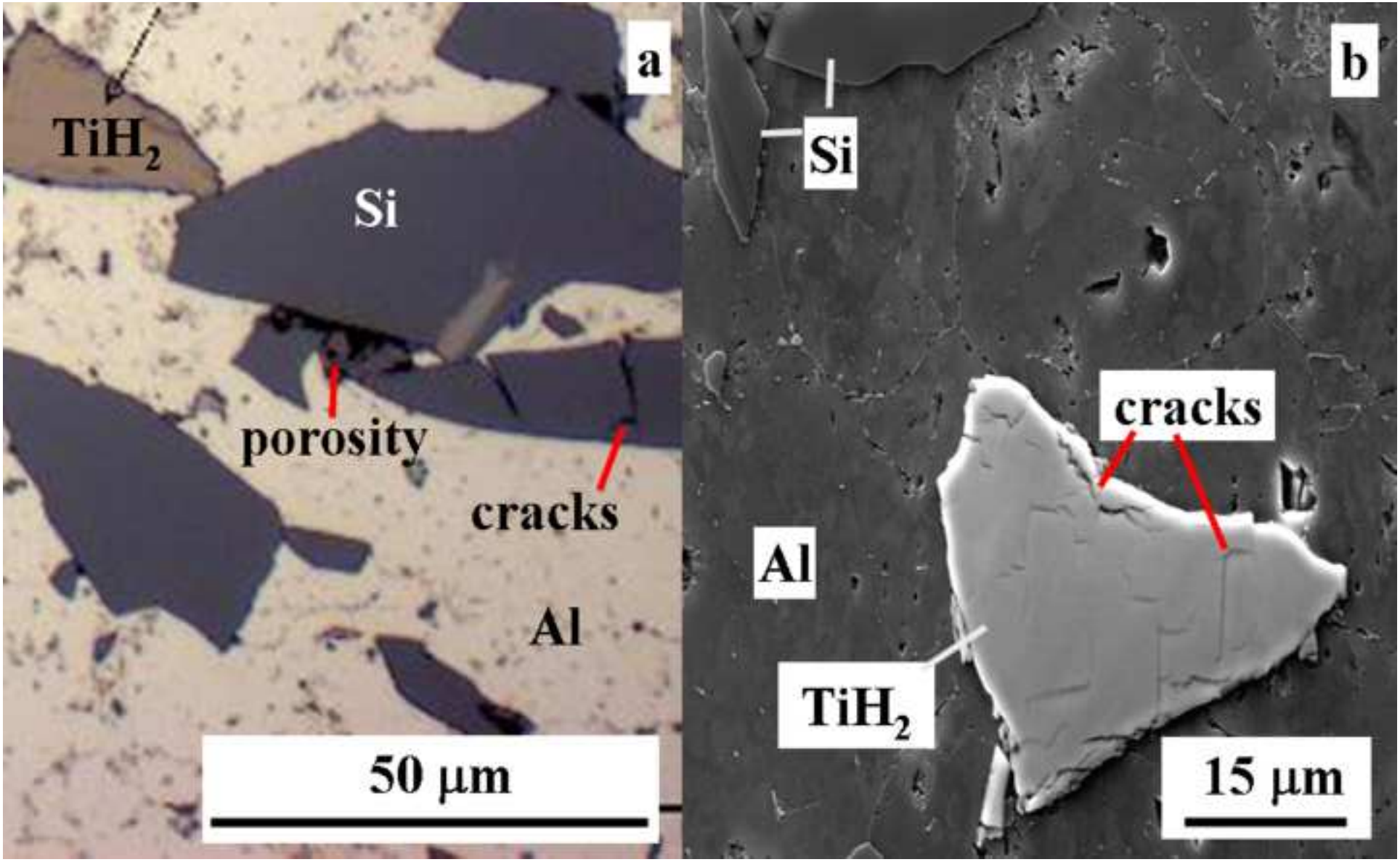

Figure(s)
Click here to download high resolution image

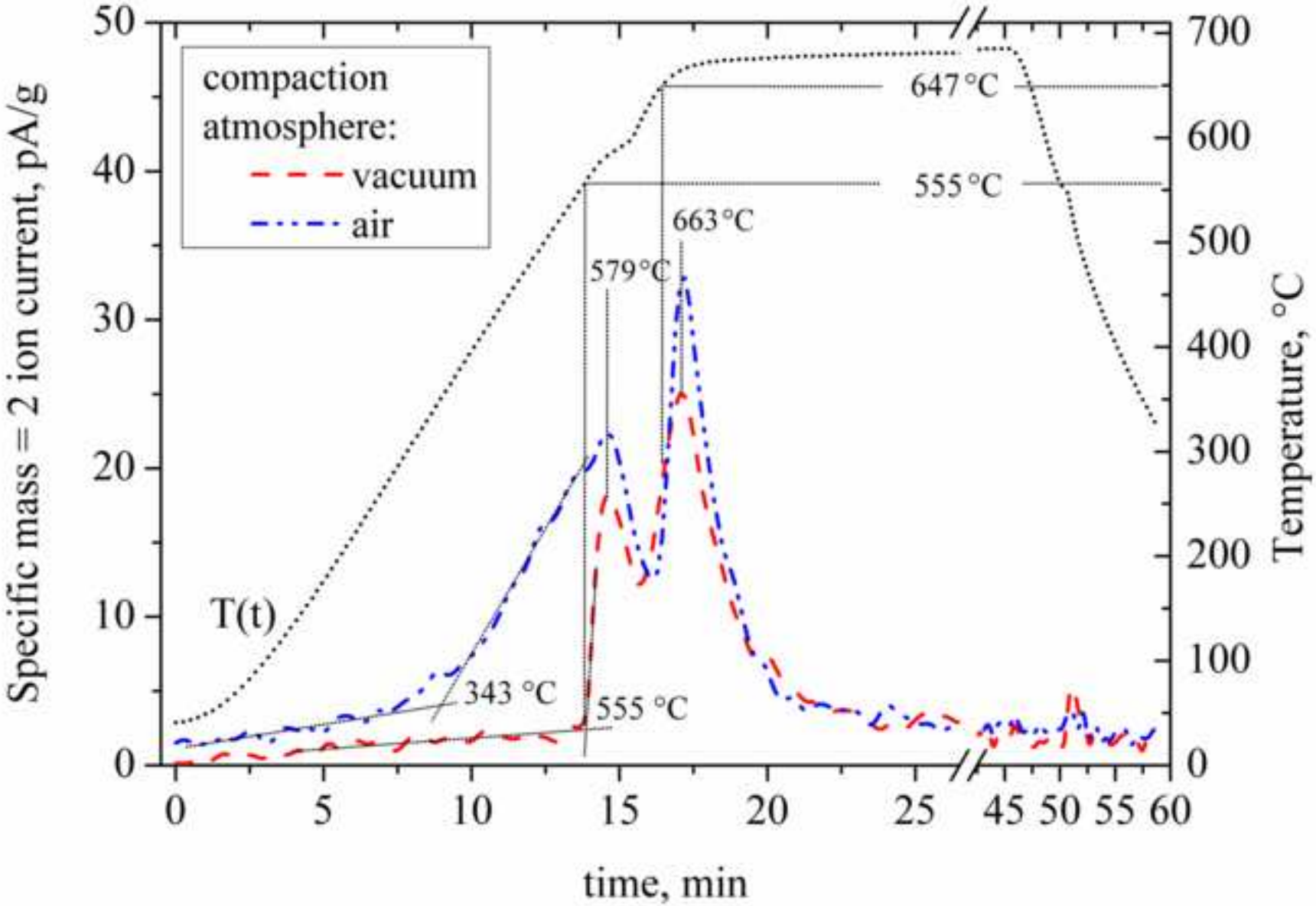

Figure(s)
Click here to download high resolution image

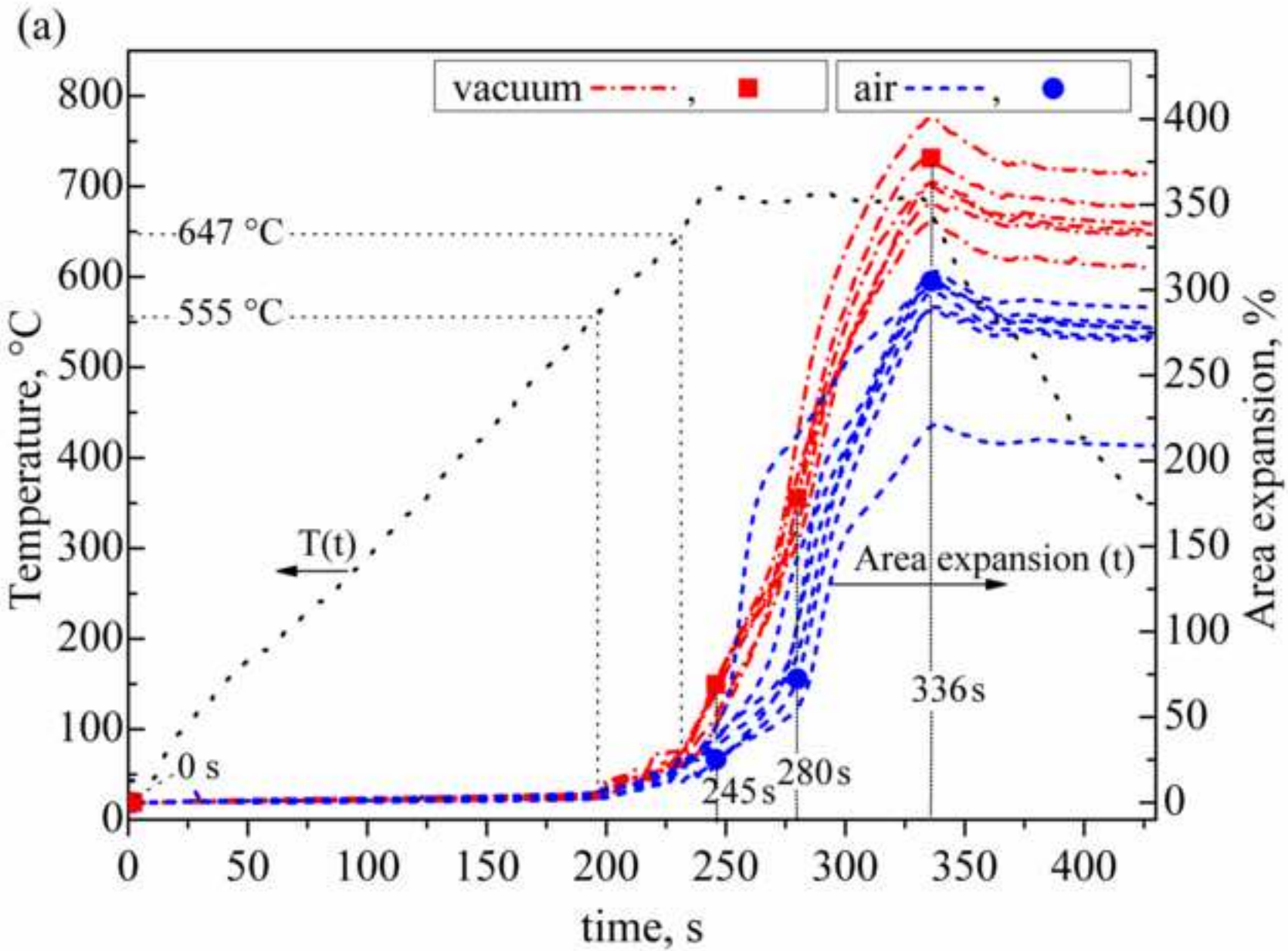

Figure(s)
Click here to download high resolution image

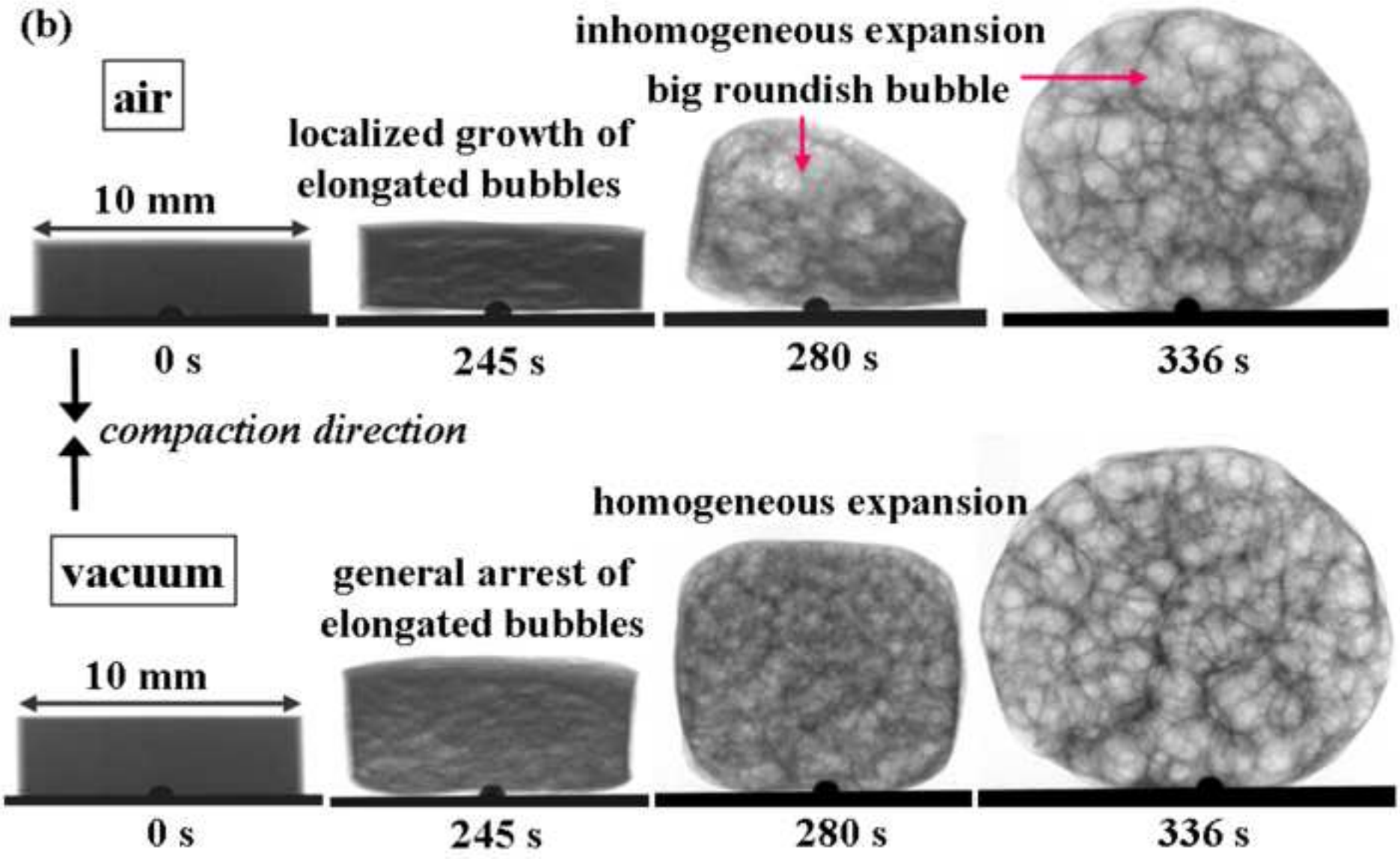

Figure(s)
Click here to download high resolution image

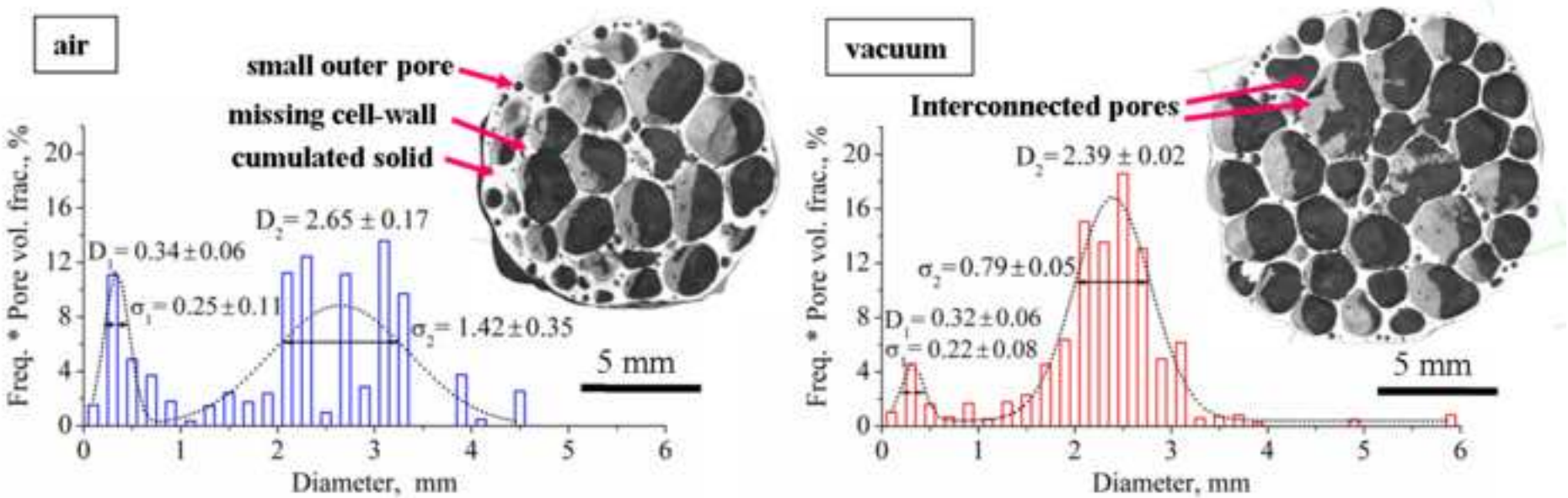

Table(s)

Fig. 1. Microstructure of compacted precursor material. a) Light microscopy image, b) SEM image.

Fig. 2. Specific mass = 2 ion current (hydrogen release) vs. time for precursor materials either compacted in air or under vacuum. The experiments were carried out in flowing synthetic air applying the temperature profile T(t). Indicated onset and peak temperatures are discussed in the text, 555 °C and 647 °C are also denoted in Fig. 3 a.

Fig. 3. a) Area expansion vs. time for 12 foams. Legends indicate the compaction atmosphere. All the samples were foamed applying the temperature profile T(t). The temperatures 555 °C and 647 °C (also marked in Fig. 2) denote the onset of non-linear expansion in the solid state and the begin of continuous expansion in the semi-molten state for the vacuum-pressed powder compacts. b) Radioscopic image sequences of representative foams at times 0, 245, 280 and 336 s labelled in a) with full-circle and full-square symbols.

Fig. 4. 3D pore size distributions of foams made from air- and vacuum-pressed precursors. Frequency × pore volume fractions as function of diameter were fitted by a double-peak Gaussian model (dotted curves). Values indicate mean diameters D_i and standard deviations σ_i for every peak. Top-right, tomographic reconstructions of central sections perpendicular to the compaction direction.

Table 1 – Properties of powder compacts

Compaction atmosphere	Oxygen content [wt.%]	Rel. density* [%]
vacuum	0.48 ± 0.05	99.24 ± 0.07
air	0.67 ± 0.08	98.93 ± 0.03

(*) relative to 2.68 gcm^{-3}, theoretical full density.